Implementation of Broadband Microwave Arbitrary-Order Time Differential Operators Using a Reconfigurable Incoherent Photonic Processor

Yongwoo Park, Member, IEEE
Mohammad H. Asghari, Student Member, IEEE
Robin Helsten
José Azaña, Member, IEEE

Implementation of Broadband Microwave Arbitrary-Order Time Differential Operators Using a Reconfigurable Incoherent Photonic Processor
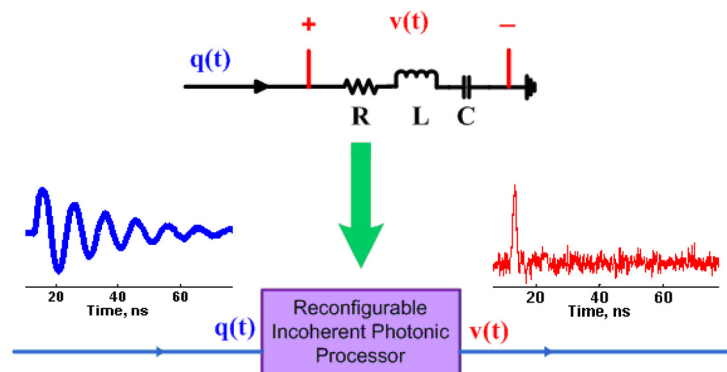
Yongwoo Park, *Member, IEEE,* **Mohammad H. Asghari,** *Student Member, IEEE,*
Robin Helsten, and **José Azaña,** *Member, IEEE*

Institut National de la Recherche Scientifique—Energie, Matériaux et
Télécommunications (INRS-EMT), Montréal, QC H5A 1K6, Canada

Abstract: A reconfigurable photonic signal processing system for arbitrary-order temporal differentiation of broadband microwave waveforms, with bandwidths up to a few tens of gigahertz, is proposed and experimentally demonstrated. This technique enables full programmability of the differentiation operator to be applied on the input microwave signal, including any desired linear differential-equation operator, by suitably reshaping the incoherent power spectrum according to the corresponding finite-difference time-domain (FDTD) equations obtained from the Euler's approximation. Successive photonic time derivatives of Gaussian-like pulse intensity waveforms with pulse widths of 42 and 72 ps were accurately achieved up to the second and the fourth order, respectively, using the same photonic processing platform. A more general operator, conceived to directly emulate the second-order differential-equation modeling a high-frequency series resistor, inductor, and capacitor (RLC) circuit, was also implemented and successfully tested.

Index Terms: Fiber optics systems, optical communications, microwave photonics signal processing.

1. Introduction

Photonic differentiators are basic building blocks for all-optical signal processing and computing capable of overcoming the processing speed limitations of equivalent conventional electric circuits. Reported photonic differentiation methods can be classified by the type of signals to be differentiated: complex (amplitude and phase) temporal envelope of the input optical signal [1]–[9] (coherent processing) or intensity time waveform [10]–[12] (incoherent processing). First-order and higher order differentiators of complex optical signals have been successfully demonstrated [1]–[9]; coherent differentiation has shown to be of scientific and practical significance for a wide range of applications, including generation of high-order Hermite–Gaussian pulse waveforms [1]–[12], ultrashort pulse shaping [13]–[15], and direct phase reconstruction of arbitrary optical signals [16]–[18]. On the other hand, incoherent photonic differentiators, operating on intensity time waveforms, have proven particularly useful for ultrawideband (UWB) microwave signal generation and processing [10]–[12], [19]–[21]. These last types of photonic differentiators can be considered as a direct all-optical

equivalent to conventional electronic temporal differentiators since amplitude-only signals are actually processed in the electronic domain. This is potentially important to ensure full compatibility with electronic solutions in future photonic-based ultrahigh-speed information processing and computing applications.

Previous methods for first-order intensity signal differentiation are generally based on discrete-time "incoherent" optical processing in which two narrow-line light sources at different wavelengths are modulated by the input waveform using a mechanism [e.g., wavelength-conversion techniques such as cross-gain modulation (XGM) in a semiconductor optical amplifier (SOA)] that provides an inversely modulated copy of the input signal at one of the wavelengths and an exact copy of this original signal at the other wavelength. Both copies are then relatively delayed in time and combined incoherently, resulting in a first-order temporal derivative of the original signal [11], [19], [21]–[23].

High-order intensity differentiation (HOD) is also of significant interest for a range of applications, such as reconfigurable UWB pulse shaping based on the combination of differently weighted HODs [14] and implementation of arbitrary differential equation operators. The latter application is particularly interesting because one could for instance implement differential operators modeling the behavior of ultrahigh-frequency resistor, inductor, and capacitor (RLC) processing circuits. This equivalence could be exploited in many different ways. For instance, classical filter design methods could be directly used for designing microwave photonic filters, e.g., aimed at realizing different signal processing functionalities on microwave signals.

In this paper, we discuss and demonstrate the design of a reconfigurable incoherent optical signal processing system aimed to implement arbitrary differential equation operators; we show that any differential operator, including first- and high-order time differentiators, can be implemented using the same programmable platform. Similar schemes, based on discrete-time microwave photonic filters, have been previously demonstrated for high-order UWB microwave pulse generation [19]–[24]. Previous experiments, however, were focused on the implementation of first- and high-order differentiators of temporal intensity waveforms; our work here represents a conceptual generalization of these previously introduced ideas by showing that conventional microwave-photonic filtering schemes can be used to implement any desired arbitrary differential equation operator. Targeting the implementation of a fully reconfigurable photonic signal processing platform [24], we propose the use of a discrete-time microwave photonic filtering scheme [25], [26] in which the desired differentiation operator can be embedded in the source power spectrum as determined by the corresponding finite-difference time-domain (FDTD) equations based on the well-known Euler approximation [27]. We note that a backward time-difference scheme based on the Taylor's series expansion has been previously used for coherent temporal differentiation [2] and that both are commonly used approaches for approximating the differentiations of a given temporal function. The successive photonic time derivatives of Gaussian-like pulse intensity waveforms as short as 40 ps [full-width-at-half-maximum (FWHM)] are demonstrated up to the fourth order using the same processing platform, which exhibits an effective processing bandwidth exceeding tens of gigahertz. Finally, a linear "second-order differential operator" conceived to emulate a high-frequency series RLC circuit is also implemented and successfully tested.

2. Operation Principle

2.1. Photonics Time Derivative Method Based on the Time–Frequency Convolution

The starting point of our proposed method is based on the generation of incoherent time-delayed bipolar copies of the original input intensity to perform the HODs of this input waveform using the FDTD approximation. The simplest central-division difference equations for first- and high-order time differentiation of an intensity signal $f(t)$ are the following [27]:

$$\frac{\partial f(t)}{\partial t} \cong \frac{f(t-h) - f(t+h)}{2h} \tag{1a}$$

$$\frac{\partial^2 f(t)}{\partial t^2} \cong \frac{f(t-2h) - 2f(t) + f(t+2h)}{4h^2} \tag{1b}$$

$$\frac{\partial^3 f(t)}{\partial t^3} \cong \frac{f(t-3h) - 3f(t-h) + 3f(t+h) - f(t+3h)}{8h^3} \tag{1c}$$

$$\frac{\partial^4 f(t)}{\partial t^4} \cong \frac{f(t-4h) - 4f(t-2h) + 6f(t) - 4f(t+2h) + f(t+4h)}{16h^4} \tag{1d}$$

where h is the time step in the Euler's approximation and essentially determines the processing bandwidth of the platform ($\propto 1/h$). A smaller value of h translates into a larger processing bandwidth and the associated reduced processing error. It is important to note that in the photonics-based implementation proposed here, the time differentiation operation does not include the denominators shown in (1a)–(1d). For example, the result of first-order intensity differentiation using the proposed photonics scheme is actually equal to $2h\gamma(\partial f/\partial t)$, where γ is the insertion loss of the differentiator. These different proportionality constants need to be taken into account when an arbitrary differential operator comprising different derivative orders is constructed. A relevant example will be discussed in the next section.

The above difference equations can be mathematically expressed as a convolution of the input intensity signal with a discrete-time finite-impulse-response (FIR) filter, as follows:

$$\frac{\partial^n f(t)}{\partial t^n} \propto f(t) \otimes \left\{ \sum_i p_i \delta(t+hi) \right\} \tag{2}$$

where p_i is the (positive or negative) weight of the successive impulse-response terms, i is an integer with an absolute magnitude smaller than n (differentiation order), $\delta(t)$ is the Kronecker delta, and $\otimes$ denotes convolution. The filter weights are determined by the factors of the target difference equation, as defined in (1). The convolution operation in (2) can be implemented using incoherent bipolar superposition of time-delayed copies of $f(t)$ [25], as shown in Fig. 1. In practice, simple time-delayed copies of the original optical signal may suffer from field interferences when they are superposed with a short time delay. One may need to use a broadband source for which the coherence length is shorter than the discrete time delay (h) [25]. Superposition of the discretely time-delayed copies at different frequencies can avoid this interference, providing incoherent addition of the discretely time-delayed intensity waveforms without any interference. A conceptual diagram for the broadband (or multiwavelength) discrete-time-delay method is shown in Fig. 1(a) (first-order differentiation is illustrated as an example). [Hereafter, this method is referred to as "the delay-line photonics microwave filter (DLMF)."] In this specific scheme, the bipolar superposition, where one electric signal is subtracted from the other electric signal in a differential amplifier, can be implemented in many alternative ways, e.g., using a 2 × 1 Mach–Zehnder electro-optic modulator (MZM) [26], a dual MZM [21], or a balanced differential photoreceiver [22], or employing XGM in an SOA [11], [19].

For reconfiguration of the filter, one can alternatively apply an equally spaced multiwavelength light source, created using a suitable reconfigurable optical filter, combined with intensity modulation of the signal to be processed and linear dispersion of the modulated light [hereafter named as "the wavelength-dispersion photonics microwave filter (WDMF)"]; see Fig. 1(b). When the modulated signal on the multiwavelength light is dispersed by applying second-order dispersion, i.e., group-velocity dispersion (GVD) ($\ddot{\Phi} = -\partial^2 \Phi/\partial \omega^2$, where $\Phi(\omega)$ is the spectral phase transfer function of a dispersive medium), e.g., by linear propagation through a highly dispersive medium such as a long section of optical fiber, each different wavelength element performs as a discrete-time-delayed copy of the modulation waveform. The time-delayed copies can then be superposed without interfering, provided that they are uncorrelated. Here, we employed a differential detection technique to implement the desired bipolar superposition (i.e., to achieve positive and negative weights), as shown in Fig. 1(b). A proper spectral filter with assigned weights p_i would allow
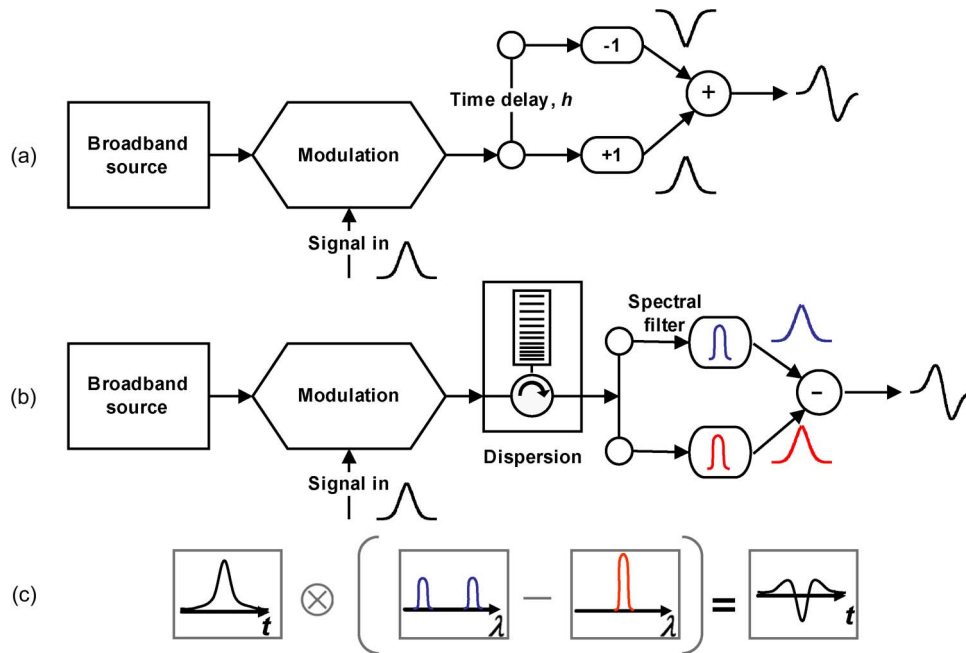
Fig. 1. Ultrafast optical signal processing for intensity time differentiation. (a) First-order time differentiation using the delay-line photonics microwave filter. (b) First-order time differentiation using the wavelength-dispersion photonics microwave filter (employed method). (c) Diagram illustrating the mathematical procedure for second-order differentiation based on incoherent processing of the time–frequency convolution.

implementing the target convolution operation, as described in (2). Reconfiguration in the spectral domain is advantageous as compared with the DLMF, considering that one just needs to simply replace or alter a spectral filter to modify the impulse response of the device.

More generally, the WDMF can be also interpreted using the time–frequency convolution concept [28]. A diagram illustrating the optical processing procedure for a second-order differentiation operation using the time–frequency convolution concept is shown in Fig. 1(c), where the output intensity profile $I_{out}(t)$ satisfies the following relation [28]:

$$I_{out}(t) \propto S(t/\ddot{\Phi}) \otimes f(t) \tag{3}$$

where S is the frequency-to-time mapped (FTM) version of the spectral energy density profile of the broadband light source. In practice, the discrete linear time delays are obtained by discretely sampling the frequency components of the dispersed incoherent pulse using a wavelength-division-multiplexing (WDM) filter. This allows one to directly setting the desired derivative weights in the spectral domain. Moreover, the sampling time h of the difference equation is directly proportional to the applied GVD, according to (3), and thus, this sampling time can be adjusted by properly fixing the GVD.

2.2. Programmable Photonics RLC Filter

To illustrate the implementation of a generalized differential-equation operator using the proposed photonics microwave filtering platform, we design and demonstrate a system emulating the lumped-element RLC circuit shown in Fig. 2. The resonance of an RLC circuit occurs when the inductive and capacitive reactances are equal in magnitude but cancel each other because they are 180° apart in phase. When the circuit is at its resonant frequency, the combined imaginary component of its admittance is zero, and hence, only the resistive component is observed [29].
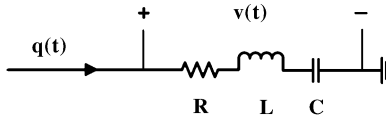
Fig. 2. Schematic of the equivalent RLC circuit emulated through the use of the proposed photonics platform.

An RLC circuit consisting of a series connection of an inductor, resistor, and capacitor (see Fig. 2) powered by an electrical charge $q(t)$, where t is the time variable, can be represented in the time domain through the differential equation [29]

$$Lq''(t) + Rq'(t) + \frac{1}{C}q(t) = v(t) \tag{4}$$

where $v(t)$ is the total electrical voltage measured along the circuit branch.

Here, we emulate this RLC circuit using a photonic incoherent processing platform that is specifically designed to implement the second-order differential operator defined by (4). Using the proposed technique, it is possible to emulate very accurately the performance of general RLC circuits over tens of gigahertz frequency bandwidths. We reiterate that the same photonic platform can be easily programmed to implement any desired arbitrary time differential operator.

The linear ordinary second-order differential equation in (4) can be rewritten in the frequency domain as follows:

$$Q(\omega) \times \left(-L\omega^2 + jR\omega + \frac{1}{C}\right) = V(\omega) \tag{5}$$

where ω is the microwave angular frequency variable. Equation (5) defines the so-called spectral transfer function of the RLC filter; assuming, for instance, that the electrical charge and voltage are considered as the input and output signals in the system, respectively, the corresponding transfer function is $H(\omega) = V(\omega)/Q(\omega) = (-L\omega^2 + jR\omega + 1/C)$. A simple way to confirm the correct operation of a designed RLC circuit is to use the inverse of the corresponding filter transfer function as the input into the filter (we assume that the filter is minimum phase, and therefore, it is invertible); in our case [29]

$$q_1(t) = \Im^{-1}\left\{\left(-L\omega^2 + jR\omega + \frac{1}{C}\right)^{-1}\right\} = Ae^{-\xi\omega_0 t}\sin(\sqrt{1-\xi^2}\omega_0 t + \phi) \tag{6}$$

where $\omega_0 = \sqrt{1/LC}$ is the resonance angular frequency, and $\zeta = 0.5R\sqrt{C/L}$ is the damping factor. A and φ are constant factors that are determined by the initial conditions. When the signal $q_1(t)$ is launched at the input of the RLC circuit, one would ideally expect to obtain a temporal Dirac-delta function at the output of the filtering circuit (the measured total voltage of the branch). This simple experiment is usually employed to confirm the correct operation of the designed circuit and will be also used here to evaluate the performance of the proposed photonics-based implementation.

In this work, we emulate the high-frequency RLC circuit described above using the microwave photonics differential technique proposed in this paper. We substitute the first- and second-order derivatives of the electrical charge parameter $q(t)$ in (4) with the equivalent discrete-time Euler's approximations given by (1). After some straightforward calculations and simplifications, we achieve the following equivalent discrete-time differential equation representing the high-frequency RLC circuit showed in Fig. 2:

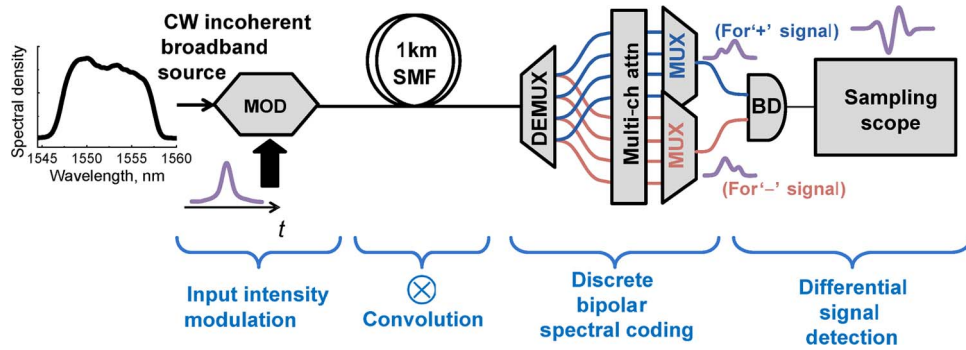$$\sum_{i=-2}^{2} p_i\, q(t+ih) = v(t) \tag{7}$$

Fig. 3. Schematic of the proof-of-concept experimental setup used for reconfigurable implementation of arbitrary temporal differential operators. The spectrum of the incoherent light source is also shown on the left. MOD: electro-optic Mach–Zehnder modulator. SMF: standard single-mode fiber. DEMUX: wavelength-division-demultiplexing filter. MUX: wavelength-division-multiplexer filter. Multi-ch attn: multi-channel attenuator. BD: differential balanced photoreceiver.

where h is the time step in the Euler's approximation (sampling time), $p_{-2} = L/4h^2$, $p_{-1} = R/2h$, $p_0 = (2h^2 - LC)/2Ch^2$, $p_{+1} = -R/2h$, and $p_{+2} = L/4h^2$. To implement the discrete-time differential equation given by (7), we rewrite the left side of (7) as a convolution of the electrical charge $q(t)$ and the temporal impulse response of a microwave photonics filter as follows:

$$v(t) = q(t) \otimes \sum_{i=-2}^{2} p_i \, \delta(t + ih). \tag{8}$$

The microwave photonics filter in (8) can be implemented using our proposed photonics time derivative method by assigning p_i values to the power weighting factors for the ith channel in the WDM filter. The processing bandwidth of the implemented high-frequency RLC filter is essentially determined by the time step in the Euler's approximation ($\propto 1/h$).

3. Experiments

For a proof-of-concept demonstration of first- and high-order intensity differentiation, successive derivatives of a Gaussian-like electric pulse were performed using the fiber-optic photonics microwave filtering setup shown in Fig. 3. A broadband incoherent CW source with a 9-nm bandwidth was prepared using the amplified spontaneous emission of an SOA followed by amplification with an Erbium-doped fiber amplifier (not shown in the setup diagram). An example of the spectrum is shown on the left side of Fig. 3. Detailed descriptions of the incoherent source preparation can be found in [28]. The CW light (average power ~15 mW) was modulated using an electro-optic Mach–Zehnder modulator (MOD) (E-O space) with a 3-dB bandwidth of 32 GHz driven by a 42-ps (FWHM), or a 72-ps Gaussian-like voltage signal. These pulse widths allowed photonic differentiation up to the second and fourth order, respectively. Different pulse widths were used with the aim of demonstrating the fastest time feature and the highest order of differentiation that the system could provide with the given configuration.

The modulated signal was subsequently dispersed through a 1-km-long standard single-mode fiber, i.e., a total GVD of ~17.3 ps/nm was applied to the modulated broadband signal. The dispersed broadband signal was split into five different wavelength channels (1549.3 nm ~ 1555.7 nm) using a WDM demultiplexer with 200-GHz (~1.6 nm in wavelength) spacing and a 0.9-nm (~112 GHz) FWHM linewidth. The used wavelength channel spacing and GVD amount fixed the sampling time constant to be $h \sim 27$ ps. The power out of each channel of the WDM demultiplexer was equally split in half via a 50/50 fiber coupler so that to achieve the desired bipolar operation.

To be more concrete, the five wavelength channels were split into two groups, respectively, corresponding to the positive and negative factors of the bipolar superposition. Hence, 10 channels
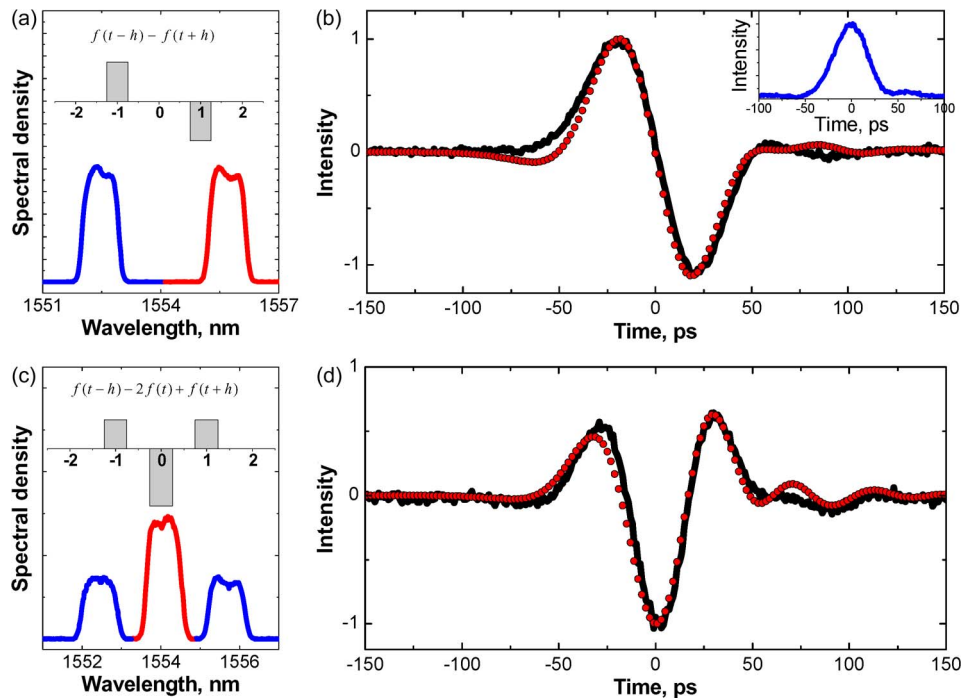
Fig. 4. First- and second-order photonic derivatives of a 42-ps (FWHM) input electric Gaussian pulse. (a) and (c) are spectral density profiles shaped according to the finite-difference codes of the first- and the second-order derivative. (b) and (d) are numerical (solid dots) and experimental curves (black lines) of the derivative outputs. The inset of (b) shows the measured 42-ps input pulse waveform.

with five different center wavelengths were prepared and attenuated individually by a variable multichannel attenuator to apply the required weights for each targeted high-order differentiation operation. Accurate temporal synchronization between channels (<5 ps in our setup) was required in order to achieve the required nearly constant time step (h, sampling time) between them. The weighting coefficients corresponding to the finite-difference approximations of the first- and second-order derivative operators [see (1a) and (1b)] were generated by properly attenuating the individual spectral channel powers. The weights for the corresponding derivatives are shown in the inset of Fig. 4(a) and (c), respectively. The weighted spectral energy density profiles for the first- and the second-order derivative are shown in Fig. 4(a) and (c), respectively, where the grouped channels corresponding to the positive (blue) and the negative (red) superposition outputs were measured using an optical spectrum analyzer (OSA).

The two spectral groups (superposed) were detected using the two inputs of a balanced differential receiver with a 3-dB bandwidth of $\sim$28 GHz (DSC-R410, Discovery Semiconductor Inc.). The average powers at each port were ranged from $\sim$5 to 10 μW, depending on the weights. Fig. 4(b) and (d) show the sampled differentiated outputs for the first- (a), and the second-order (b) derivative of the 42-ps (FWHM) input pulse. This pulse [shown in the inset of Fig. 4(b)] was generated by an opto-electronic conversion of optical pulse via a fast photodetector followed by an radio frequency (RF) amplifier; for optical pulse generation, a passively mode-locked fiber laser generated a picosecond transform-limited pulse with a repetition rate of 16.7 MHz, which was subsequently dispersed through a 1-km standard single-mode fiber in order to shape the optical pulse like a Gaussian function with the FWHM of 42 ps. The use of a shorter optical pulse would have induced an undesired ringing profile of the opto-electronically converted electric pulse due to the impulse response characteristics of the fast photodetector. Numerical differentiations of the input intensity pulse (solid circles) are also given for direct comparison. Offset and rescaling were performed to properly compare the measurement results with the numerical differentiations, clearly
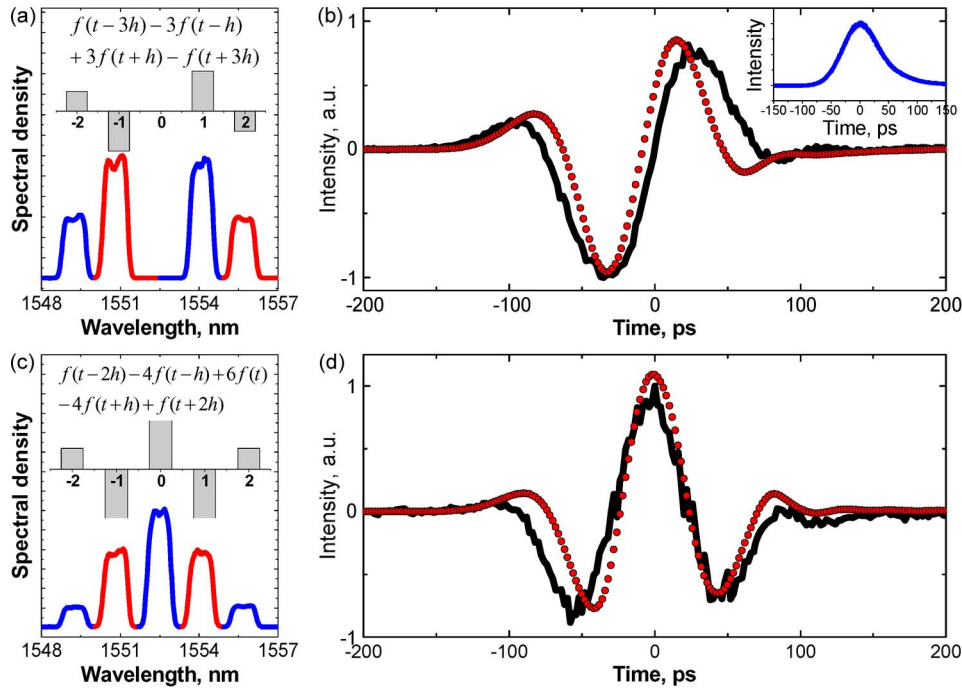
Fig. 5. Third- and fourth-order photonics derivatives of a 72-ps (FWHM) input electric Gaussian pulse. (a) and (c) are spectral density profiles shaped according to the finite-difference codes of the third- and the fourth-order derivatives. (b) and (d) are numerical (solid dots) and experimental curves (black lines) of the derivative outputs. The inset of (b) shows the measured 72-ps input pulse waveform.

showing excellent agreement between the simulations and the experiments. Higher than second-order derivatives were not successfully generated as there were clear discrepancies between the numerical and the experimental curves (not presented here). This can be partly attributed to the long temporal duration ($\sim$110 ps) of the spectrally weighted derivative operator compared with the applied input pulse width ($\sim$42 ps, FWHM); in other words, h was too long to differentiate the given input pulse at the third order accurately. In order to demonstrate accurate derivatives for higher than second order, a 72-ps (FWHM)-long pulse was prepared in which a dispersed optical pulse was opto-electronically converted into an electric pulse by use of a high-speed photodiode followed by an RF amplifier. A similar procedure to that described above was then implemented to spectrally weight the different wavelength channels to achieve the target third- and fourth-order derivatives. The results, which are shown in Fig. 5, clearly prove that the experimentally achieved output temporal profiles agreed well with the numerical estimations.

As a final experimental test, in order to illustrate the capability of the proposed method to implement fully arbitrary time differential operators, we demonstrated a second-order differential equation operator, comprising a combination of first- and second-order time derivatives. In this experiment, we targeted to emulate the second-order differential equation modeling the series RLC circuit introduced in Section 2.2. Said another way, we targeted to emulate a high-frequency RLC electronic circuit such as that shown in Fig. 2 with the following parameters: $R = 0.2\ \Omega$, $L = 1$ nH, and $C = 2.5$ nF. This corresponds to a high-frequency second-order RLC filter with a resonance angular frequency of $\sim 0.632 \times 10^9$ rad/s and a damping factor of ~ 0.16. The frequency-domain equation corresponding to such an RLC filter (see (5) above) is

$$Q(\omega) \times (-\omega^2 + j0.2\omega + 0.4) = V(\omega) \tag{9}$$

where $\omega = 2\pi f$ and f is the frequency in gigahertz. The relative weighting factors for the input signal and its first- and second-order derivates were 0.4, 0.2, and 1, respectively. As described in
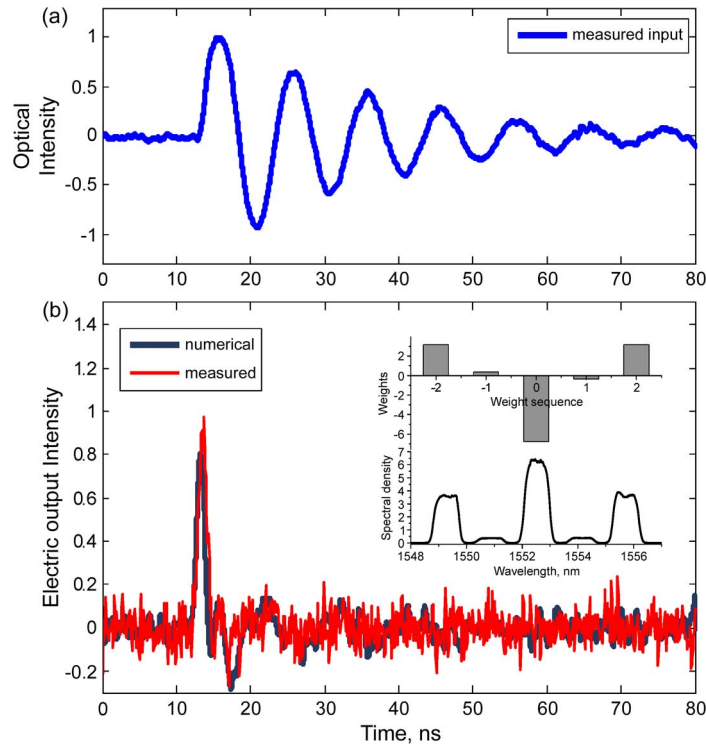
Fig. 6. (a) Measured input modulation signal. (b) Measured output waveform (red curve) after the photonics RLC filter. A numerical differentiation (black curve) of the input signal with the RLC filter operator is also shown for comparison.

Section 2.2, this high-frequency RLC filter can be implemented using the discrete-time filtering scheme with the impulse response defined in (8), with the following p_i values:

$$p_{-2} \approx 0.25, \quad p_{-1} \approx 0.1 \times 10^9 h, \quad p_0 \approx 0.4 \times 10^9 h - 0.5, \quad p_{+1} \approx -0.1 \times 10^9 h, \quad p_{+2} \approx 0.25 \quad (10)$$

where h is the time step in the Euler's approximation in nanoseconds. We used the same WDM filters (MUX and DEMUX in Fig. 3) as we used for the previous experiment, and the length of the single-mode fiber section used for dispersion was ~10.5 km. These parameters define a time step in the Euler's approximation of $h \approx 0.28$ ns. This gives the following relative weighting factors (normalized to p_{+1}) for the power of the different channels in the multiwavelength attenuator (see Fig. 3):

$$p_{-2} \approx 8.3, \quad p_{-1} \approx 1, \quad p_0 \approx -13, \quad p_{+1} \approx -1, \quad p_{+2} \approx 8.3. \quad (11)$$

The corresponding testing input waveform (leading to the generation of a temporal delta at the system output) is (see (6) above)

$$q_1(t) = Ae^{-0.1t}\sin(0.62\ t) \quad (12)$$

where t is the time variable in nanoseconds. The input testing waveform given by (12) was electrically generated using an arbitrary waveform generator (Tektronics Inc., AWG710B) with a sampling rate of 4 GS/s (gigasamples per second). The generated electric waveform is shown in Fig. 6(a). This waveform modulated CW light over an optical bandwidth of ~9 nm. The modulated light was subsequently dispersed in a 10.5-km-long section of standard single-mode fiber, leading to a corresponding time delay between the neighbor channels of ~0.28 ns. In order to spectrally weight the reconfigurable WDM filter to implement the target second-order differential equation operator, five weighting factors were implemented using the multichannel attenuator, as defined by

(11). In this case, the fastest time features were limited by the sampling rate of the waveform generator. A relatively large time step was attributed to the undesirable mismatch of the time synchronization between wavelength channels. Thus, the superposed weighting constants were calculated as $8.3 \cdot S(f_c - 2\Delta f) + 1 \cdot S(f_c - \Delta f) - 13 \cdot S(f_c) - 1 \cdot S(f_c + \Delta f) + 8.3 \cdot S(f_c + 2\Delta f)$, where S is the channel spectral transmission profile, f_c is optical frequency at the center channel, and Δf is the channel spacing ($\sim$200 GHz). After the spectral filtering with the proper weighting vector [as defined by (11)], the output spectrum was measured, and it is shown in the inset of Fig. 6(b), together with the weighting vector. The measured output intensity waveform is shown in Fig. 6(b), compared with the numerically calculated curve, demonstrating an excellent agreement with the theoretical modeling. As predicted, an impulse at the output [shown in Fig. 6(b)] was generated, and the numerical simulation (black curve) also agreed well with this impulse generation.

4. Conclusion

A multichannel incoherent photonic processing scheme for reconfigurable arbitrary-order temporal differentiation of broadband microwave signals has been proposed and experimentally demonstrated. The successive time derivatives of Gaussian-like pulse intensity waveforms with pulse widths of 42 ps (FWHM) and 72 ps (FWHM) were accurately achieved up to the second and up to the fourth order, respectively, using the same spectral filtering platform. As a generalization of this basic realization, the use of the same photonic configuration to compute any desired linear differential equation has been also proposed and demonstrated. The latter has been illustrated through the successful implementation and testing of a second-order differential-equation operator (including a combination of first- and second-order derivatives) that has been specifically designed to model the functionality of a series RLC circuit. Efficient annihilation of a properly shaped high-frequency damped harmonic oscillation function has been achieved using the emulated circuit, which is in excellent agreement with the theoretical and numerical predictions.

References

[1] N. Q. Ngo, L. N. Binh, and X. Dai, "Optical dark-soliton generators and detectors," *Opt. Commun.*, vol. 132, no. 3/4, pp. 389–402, Dec. 1996.
[2] N. Q. Ngo, S. F. Yu, S. C. Tjin, and C. H. Kam, "A new theoretical basis of higher-derivative optical differentiators," *Opt. Commun.*, vol. 230, no. 1–3, pp. 115–129, Jan. 2004.
[3] M. Kulishov and J. Azaña, "Long-period fiber gratings as ultrafast optical differentiators," *Opt. Lett.*, vol. 30, no. 20, pp. 2700–2702, Oct. 2005.
[4] R. Slavík, Y. Park, M. Kulishov, R. Morandotti, and J. Azaña, "Ultrafast all-optical differentiators," *Opt. Express*, vol. 14, no. 22, pp. 10 699–10 707, Oct. 2006.
[5] Y. Park, R. Slavík, and J. Azaña, "Ultrafast all-optical first- and higher-order differentiators based on interferometers," *Opt. Lett.*, vol. 32, no. 6, pp. 710–712, Mar. 2007.
[6] L. M. Rivas, S. Boudreau, Y. Park, R. Slavík, S. LaRochelle, A. Carballar, and J. Azaña, "Experimental demonstration of ultrafast all-fiber high-order photonic temporal differentiators," *Opt. Lett.*, vol. 34, no. 12, pp. 1792–1794, Jun. 2009.
[7] R. Slavík, Y. Park, M. Kulishov, and J. Azaña, "Terahertz-bandwidth high-order temporal differentiators based on phase-shifted long-period fiber gratings," *Opt. Lett.*, vol. 34, no. 20, pp. 3116–3118, Oct. 2009.
[8] M. A. Preciado, V. Garcia-Muñoz, and M. A. Muriel, "Ultrafast all-optical Nth-order differentiator based on chirped fiber Bragg gratings," *Opt. Express*, vol. 15, no. 12, pp. 7196–7201, 2007.
[9] M. Li, D. Janner, J. Yao, and V. Pruneri, "Arbitrary-order all-fiber temporal differentiator based on a fiber Bragg grating: Design and experimental demonstration," *Opt. Express*, vol. 17, no. 22, pp. 19 798–19 807, 2009.
[10] J. Xu, X. Zhang, J. Dong, D. Liu, and D. Huang, "High-speed all-optical differentiator based on a semiconductor optical amplifier and an optical filter," *Opt. Lett.*, vol. 32, no. 13, pp. 1872–1874, Jul. 2007.
[11] J. Xu, X. Zhang, J. Dong, D. Liu, and D. Huang, "All-optical differentiator based on cross-gain modulation in semiconductor optical amplifier," *Opt. Lett.*, vol. 32, no. 20, pp. 3029–3031, Oct. 2007.
[12] Z. Li and C. Wu, "All-optical differentiator and high-speed pulse generation based on cross-polarization modulation in a semiconductor optical amplifier," *Opt. Lett.*, vol. 34, no. 6, pp. 830–832, Mar. 2009.
[13] Y. Park, M. Kulishov, R. Slavík, and J. Azaña, "Picosecond and sub-picosecond flat-top waveform generation using uniform long-period fiber gratings," *Opt. Express*, vol. 14, pp. 12 670–12 678, 2006.
[14] M. H. Asghari and J. Azaña, "Proposal and analysis of a reconfigurable pulse shaping technique based on multi-arm optical differentiators," *Opt. Commun.*, vol. 281, no. 18, pp. 4581–4588, Sep. 2008.
[15] R. Slavík, Y. Park, and J. Azaña, "Long-period fiber-grating-based filter for generation of picosecond and subpicosecond transform-limited flat-top pulses," *IEEE Photon. Technol. Lett.*, vol. 20, no. 10, pp. 806–808, May 2008.

[16] F. Li, Y. Park, and J. Azaña, "Complete temporal pulse characterization based on phase reconstruction using optical ultrafast differentiation (PROUD)," *Opt. Lett.*, vol. 32, no. 22, pp. 3364–3366, Nov. 2007.

[17] F. Li, Y. Park, and J. Azaña, "Single-shot real-time frequency chirp characterization of telecommunication optical signals based on balanced temporal optical differentiation," *Opt. Lett.*, vol. 34, no. 18, pp. 2742–2744, Sep. 2009.

[18] F. Li, Y. Park, and J. Azaña, "Linear characterization of optical pulses with durations ranging from the picosecond to the nanosecond regime using ultrafast photonic differentiation," *J. Lightw. Technol.*, vol. 27, no. 21, pp. 4623–4633, Nov. 2009.

[19] Q. Wang, F. Zeng, S. Blais, and J. Yao, "Optical ultrawideband monocycle pulse generation based on cross-gain modulation in a semiconductor optical amplifier," *Opt. Lett.*, vol. 31, no. 21, pp. 3083–3085, Nov. 2006.

[20] S. Pan and J. Yao, "Optical generation of polarity- and shape-switchable ultrawideband pulses using a chirped intensity modulator and a first-order asymmetric Mach–Zehnder interferometer," *Opt. Lett.*, vol. 34, no. 9, pp. 1312–1314, May 2009.

[21] M. Bolea, J. Mora, B. Ortega, and J. Capmany, "Optical UWB pulse generator using an N tap microwave photonic filter and phase inversion adaptable to different pulse modulation formats," *Opt. Express*, vol. 17, no. 7, pp. 5023–5032, Mar. 2009.

[22] Q. Wang and J. Yao, "Switchable optical UWB monocycle and doublet generation using a reconfigurable photonic microwave delay-line filter," *Opt. Express*, vol. 15, no. 22, pp. 14 667–14 672, Oct. 2007.

[23] P. Velanas, A. Bogris, A. Argyris, and D. Syvridis, "High-speed all-optical first- and second-order differentiators based on cross-phase modulation in fibers," *J. Lightw. Technol.*, vol. 26, no. 18, pp. 3269–3276, Sep. 2008.

[24] Y. Park, M. H. Asghari, and J. Azaña, "Reconfigurable higher-order photonic intensity temporal differentiator," in *Proc. IEEE LEOS Annu. Meeting*, Belek-Antalya, Turkey, Oct. 4–8, 2009, pp. 731–732.

[25] J. Capmany, B. Ortega, D. Pastor, and S. Sales, "Discrete-time optical processing of microwave signals," *J. Lightw. Technol.*, vol. 23, no. 2, pp. 702–723, Feb. 2005.

[26] J. Capmany, J. Mora, D. Pastor, and B. Ortega, "High-quality online-reconfigurable microwave photonic transversal filter with positive and negative coefficients," *IEEE Photon. Technol. Lett.*, vol. 17, no. 12, pp. 2730–2732, Dec. 2005.

[27] D. V. Griffiths and I. M. Smith, *Numerical Methods for Engineers*. Boca Raton, FL: CRC, 2006.

[28] Y. Park and J. Azaña, "Optical signal processors based on time-spectrum convolution," *Opt. Lett.*, vol. 35, no. 6, pp. 796–798, Mar. 2010.

[29] J. W. Nilsson and S. Riedel, *Electric Circuits,* 8th ed. Englewood Cliffs, NJ: Prentice-Hall, 2007.